Uniform high spectral resolution demonstrated in arrays of TES x-ray microcalorimeters

Caroline A. Kilbourne[a], Simon R. Bandler[a,b], Ari -D. Brown[a,f], James A. Chervenak[a],
Enectali Figueroa-Feliciano[a,c], Fred M. Finkbeiner[a,d], Naoko Iyomoto[a,e], Richard L. Kelley[a],
F. Scott Porter[a], and Stephen J. Smith[a,f]

[a]NASA/Goddard Space Flight Center, Greenbelt, MD 20771, USA;
[b]CRESST and University of Maryland, College Park, MD 20742, USA;
[c]Massachusetts Institute of Technology, Cambridge, MA 02139, USA;
[d]RS Information Systems Inc., McLean, VA 22102, USA;
[e]Johns Hopkins University, Physics and Astronomy Dept., Baltimore, MD 21218, USA;
[f]NASA Postdoctoral Program Resident Research Associate

ABSTRACT

Individual x-ray calorimeters based on superconducting transition-edge sensors (TES) have already demonstrated the spectral resolution, speed, and quantum efficiency needed for astrophysical x-ray spectroscopy. We are now beginning to realize this capability on the array scale for the first time. We have developed a new design for the x-ray absorber that has connections to the TES engineered to allow contact only in regions that do not serve as the active thermometer. We have further constrained the design so that a low-resistance absorber will not electrically short the TES, permitting the use of high-conductivity electroplated gold for the x-ray absorber. With such a well-behaved material for the absorber, we now achieve energy resolution at 6 keV in the range 2.4 - 3.1 eV FWHM in all the pixels of the same design tested in a close-packed array. We have achieved somewhat higher resolution and faster response by eliminating some of the gold and electroplating bismuth in its place. These are important steps towards the high-resolution, high-fill-factor, microcalorimeter arrays needed for x-ray astrophysics observatories such as Constellation-X.

Keywords: microcalorimeters, transition-edge sensors, Constellation-X

1. INTRODUCTION

We have been developing arrays of x-ray microcalorimeters to meet the requirements of the X-ray Microcalorimeter Spectrometer (XMS) instrument on Constellation-X, a future x-ray observatory under formulation by NASA. The XMS focal plane requirements stipulate a 5 arcmin × 5 arcmin field of view sampled at 5 arcsec. The highest spectral resolution, 2.5 eV, is required of the central quarter of the array, or 2.5 arcmin × 2.5 arcmin. The required spectral resolution of the rest of the array is 8 eV at 6 keV and below. Our plan to meet these requirements is to fill the focal plane with a combination of a high-performance core array and a field-of-view extension. The core array is a 32×32 array of 5-arcsec, independent microcalorimeters. Each pixel consists of a superconducting transition-edge sensor (TES) that acts as the calorimeter thermometer, an x-ray absorber, and a silicon-nitride membrane thermal link to the 50 mK heat sink. The absorber is larger than the TES and its thermal link, making thermal contact to the TES but elsewhere extending cantilevered above the sensor plane by several microns. The size of the gap between adjacent absorbers thus can be on the scale of 5 μm. For the field of view extension, which has three times the number of spatial elements as the core array, the spectral resolution and speed of the additional elements are relaxed relative to the core array. This extension will be useful for studies of dark matter and energy, where measurements of the x-ray emitting gas on large scales in clusters is needed. Our microcalorimeter array development thus far has concentrated on demonstrating an energy resolution of 2.5 eV FWHM at 6 keV, in an array of pixels with better than 95% quantum efficiency (QE) at 6 keV, to meet the requirements of the core array. Here we report on our progress in this development.
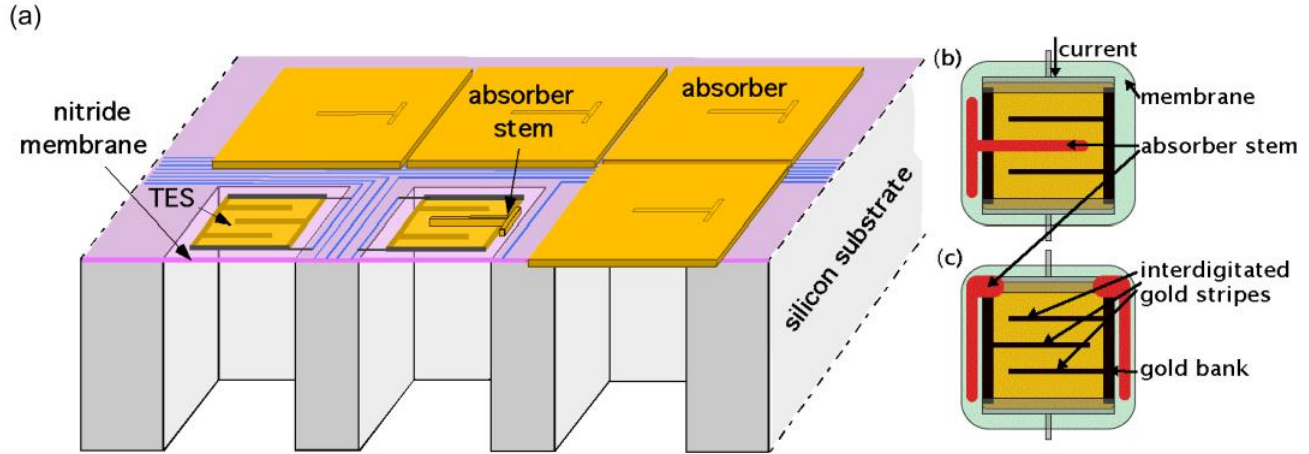
Figure 1. (a) Illustration of x-ray absorbers and their contacts. The front-left pixel shows the TES without an absorber and the middle front shows the part of the absorber that is in contact with the TES. In this example, the absorber is supported by a stem that is shaped like a "T". (b) Overhead view of the stem and TES design for a "T" shaped stem. (c) Alternative "J" shaped stem that contacts the TES at only one of the electrical contacts.

We have been producing 8×8 TES arrays with a pitch of 0.25 mm. The TES thermometer is a Mo/Au bilayer with a superconducting transition temperature, T_c, of ∼0.1 K. Each is 0.14 mm wide, allowing room for routing the sensor wiring underneath overhanging close-packed absorbers as shown in Fig. 1. Atop the bilayer we pattern additional Au features. Banks of thick Au are put along the edges parallel to the current flow to define the superconducting boundary condition and make the transition shape more uniform than if the superconducting boundary were etch-defined. Interdigitated gold stripes are oriented perpendicularly to the current flow, which has been shown to diminish the excess white noise associated with TES devices.[1] Initially we deposited x-ray absorbers directly on top of the TES thermometers,[2] limiting the first layer of the absorber to a material that would not alter the properties of the TES itself nor shunt current away from it. We used evaporated bismuth for the first layer, which has a sufficiently low electron density that it does not alter the superconducting transition of the underlying Mo/Au bilayer (in the absence of chemical interaction). It also has sufficiently poor electrical conductivity that significant shunting of the current was avoided. On top of the bismuth we deposited a layer of copper to tune the heat capacity and to provide a continuous, highly conducting layer to enhance thermal diffusion across the absorber. Finally, a top layer of bismuth was deposited that was thick enough to provide the required QE. Although a resolution of ∼2 eV FWHM was predicted from models and the measured signal and noise, the best resolution achieved using this design was 4.4 eV at 6 keV.[2] This result suggested that variations in the transport of energy across the loosely packed Bi grains to the thermalizing Cu layer was limiting the resolution despite the adequate diffusivity of the Cu layer. This absorber design was also vulnerable to interdiffusion and the formation of intermetallics at the interface with the TES, leading to alteration of the TES transition in an uncontrolled manner, further degrading the performance.[2]

In our new design[2] there is no direct contact between the absorber and the superconducting regions of the thermometer; the absorber makes contact only at normal-conducting features that are already part of the sensor design and is suspended over the active regions of the thermometer. The basic geometry is shown in Fig. 1(a). In one approach, shown in Fig. 1(a-b), the supporting "stem" of the absorber takes the shape of a "T", with a narrow bar forming the central normal-metal stripe of the TES and a second bar touching the membrane, perpendicular to the first, that provides mechanical stability without shunting current away from the TES. We also analyzed a "J" geometry, as depicted in Fig. 1(c), in which the absorber touches only the membrane and the Au banks on either side of the TES, and an "H" (shown only in the photograph of Fig. 2(a)) in which a central contact extends completely across the TES, connecting with on-membrane supports on either side. This new design scheme enables deposition of a highly conducting metal as the first layer in the absorber, or even as the entire absorber.
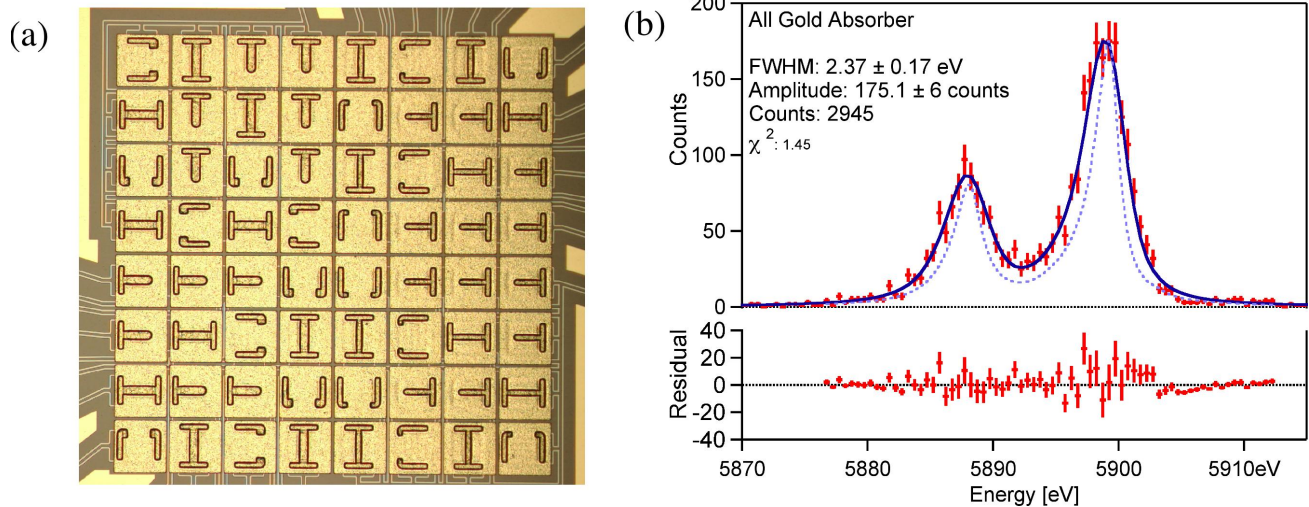
Figure 2. (a) Photograph of an 8×8 array of all-gold absorbers. The array includes "T", "J" and "H" shaped stems. (b) Spectrum of Mn K$_\alpha$ x-rays from a pixel with a "T"-shaped stem and a 4 μm thick gold absorber. The instrumental function is consistent with a Gaussian response and a resolution of 2.4 eV FWHM. The dashed line shows the intrinsic line shape from Hölzer et al.,[3] with correction and extension provided by Hölzer via private communication.

2. GOLD ABSORBERS

2.1 Array design and performance

The most extreme application of the new absorber designs is to make the absorbers with solid electroplated gold. The advantages of this approach are that the physical properties of gold are well understood and that electroplating is able to produce gold films with very high conductivity. Such a well-behaved absorber would be expected to produce microcalorimeters with uniform, reproducible, and easily modeled performance. Even the somewhat non-ideal aspect of the new absorber design, having absorber supports that touch the membrane outside of the TES, is rendered negligible by such an absorber with a fast internal equilibration time. The only consideration is whether the heat capacity of a gold absorber thick enough to achieve the required QE is compatible with the resolution requirement. For the XMS pixel size and the characteristics of the superconducting transition of our typical TES thermometers, a solid gold absorber has sufficiently low heat capacity for $T_c <$ 0.09 K. On TES devices with Mo/Au bilayers and three interdigitated Au stripes (as shown in Fig. 1) we typically have an α of $\sim$100 (where $\alpha=(T/R)\mathrm{d}R/\mathrm{d}T$ characterizes the steepness of the transition) at a bias point of 15% of the normal resistance. We typically achieve the highest signal-to-noise ratio at this bias point. Depositing 6 keV of energy in a gold absorber at 0.087 K (1.4 pJ/K heat capacity) will cause the resistance of such an optimally biased TES to double.[4] While that appears to leave a lot of dynamic range above 6 keV before the normal resistance is reached, the response becomes highly non-linear long before the onset of normal-state saturation, because the signal current scales as the reciprocal of the resistance. A conservative rule of thumb is to define the linear range as extending from the bias resistance to a resistance twice that starting point. By that criterion, a gold absorber is an ideal match to our standard TES at 0.09 K.

We have fabricated 8x8 arrays of TES pixels with 4-μm gold absorbers that were electroplated on thin evaporated seed layers.[5] A picture of one of these arrays is shown in Fig 2(a). With such arrays we routinely obtain better than 3 eV resolution at 6 keV, with the best measured result being 2.4 ± 0.2 eV, as shown in Fig. 2(b). This spectrum was acquired with a heat sink temperature of 0.05 K, and with a TES transition temperature of 0.088 K. A simple calorimeter model with parameters that fit complex impedance[6] and current-voltage measurements of these devices predicts a resolution of 2.3 eV.[4]

We have measured 13 pixels of the "T" and "J" types and found the energy resolution to be better than 3.1 eV in all pixels. In some of these pixels we observed some broadening of the MnK$_\alpha$ x-ray lines that was greater that predicted from the signal and noise. This broadening can be due to variation in the TES temperature over
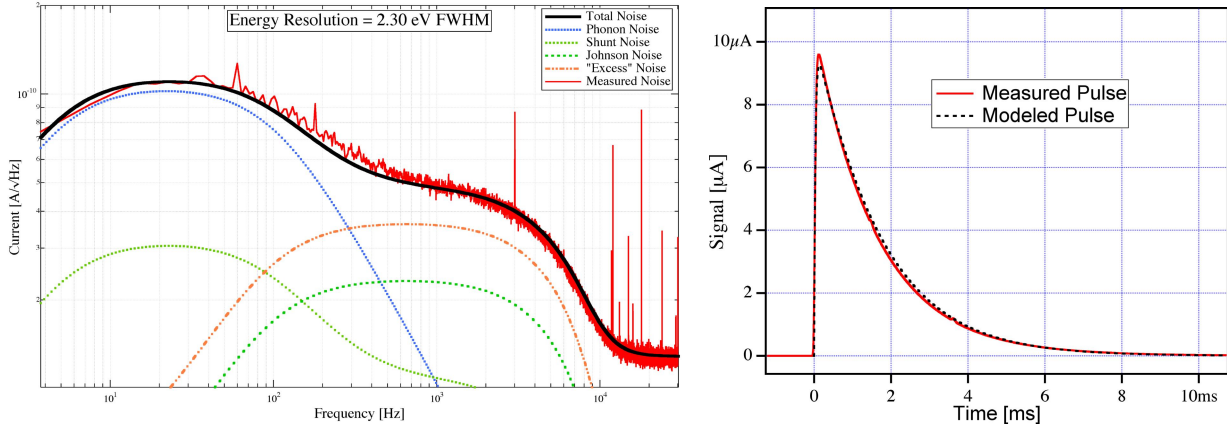
Figure 3. (left) The measured noise of a TES pixel with a gold absorber at its optimal operating point and the best fit using parameters from fitting a simple calorimeter model to complex impedance data. The main noise components that contribute to the total noise are also shown. (right) Measured pulse from a 6 keV x-ray compared with a simulated pulse using the best fit detector parameters.

the course of data acquisition. The temperature of the heat sink was kept extremely stable, with a temperature variation typically less than 100 nK rms, which would have negligible impact on the resolution. However, small variations in the thermal load on the sensors and variations in the array substrate temperature due to the absorption of x-rays on other pixels can cause broadening of the energy resolution. We also need to investigate possible variation in the gain of the electronics.

2.2 Characterization and noise

We have made detailed characterization measurements of the pixels in our 8×8 arrays of TES microcalorimeters with gold absorbers and have developed models that describe the performance well, as has been described elsewhere.[4,7] This modeling has allowed us to determine that each TES pixel is well described as a simple microcalorimeter in which the absorber thermalizes the energy of an x-ray instantaneously, and the sensor and the absorber act as a single thermal mass. Detector characterization involves a measurement of the frequency-dependent transfer function between the bias input and the output at various points throughout the superconducting transition, which is used to determine α and $\beta = (I/R)\mathrm{d}R/\mathrm{d}I$ at each point. These parameters, along with the heat capacity C, thermal conductance G, and electrical circuit parameters, can be used in a simple calorimeter model to generate simulated pulses and noise that can then be compared with the observed pulse-shapes and noise throughout the transition. An example of the success of such characterization is shown in Fig. 3. In fitting the observed noise to the model, the detector and circuit parameters are fixed, and the only free parameter is the magnitude of the so-called "excess" or "unexplained" noise[1] that dominates the noise just above the thermal signal band. At low frequencies (< 10 Hz), the noise is rolled off by a low-pass filter, and at high frequencies (> 10 kHz), after the L/R roll-off from the detector circuit, the noise is dominated by the digitization noise of the data acquisition system. As is demonstrated in this figure, both qualitatively and quantitatively our noise data match the expected noise very well, and this is true for all points in the transition. The agreement of the measurement and modeled pulse-shape is similarly very good. This agreement gives us confidence that the performance of these arrays is well understood, and our models will allow us to perform further optimization.

2.3 Thermal Conductance and Time Constant

The thermal conductance G between each pixel and the heat bath is limited by the silicon nitride membrane. From measurements of TES's on solid substrates, we have determined that the electron-phonon and Kapitza components of the conductance are much higher than the conductance in the membrane.[8] Thermal transport in the nitride membranes is quasi-ballistic because of extremely long phonon mean-free paths, as we and other groups have shown,[9,10] resulting in a thermal conductance that depends on the perimeter of the TES and the thickness of the membrane. We have measured the thermal conductance for a number of pixels with different
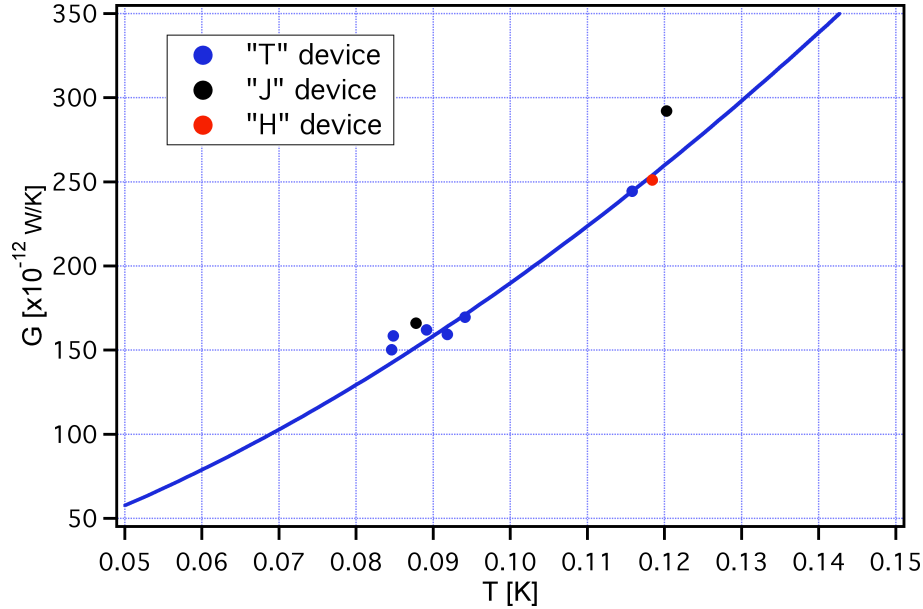
Figure 4. Measurements of the thermal conductance to the heat sink taken from 8 pixels with different stem geometries and a range of critical temperatures T_c. The line drawn through the points is representative of the temperature dependence of the thermal conductance.

stem designs, as shown in Fig. 4 and determined that there is no significant difference in the thermal conductance of these designs, in spite of the perimeter being significantly different. This is apparently because the phonons radiating out from the membrane directly below the TES in the direction of the part of the stem on the membrane will be intercepted by the nitride directly under stem that is also at the TES temperature. It is therefore only the "outer" part of the combined TES film plus stem area that will determine the thermal conductance, and this is very similar for the "T" ,"J", and "H" designs.

The recovery time constant of the pulses from the gold-absorber pixels has been ∼2 ms when operated with low circuit inductance. Increasing the circuit inductance to the point of critical damping slows the pulse rise and speeds the recovery so that the two time constants become equal, for an overall enhanced recovery time that ultimately will be used to minimize pile up.[11] (The slowed rise is also needed to enable the most effective multiplexing.[11]) Even considering this eventual speed up, we are aiming to reduce the time constant in the low-inductance limit by about a factor of 5. This time constant, τ_{eff} is determined by several parameters, including G.

$$\tau_{\text{eff}} = \frac{\left(\frac{C}{G}\right)\left(1 + \beta + \frac{R_s}{R}\right)}{\left((1 + \beta + \frac{R_s}{R}) + (1 - \frac{R_s}{R})(\frac{\alpha}{n})(1 - \frac{T_b^n}{T^n})\right)} , \qquad (1)$$

where R and R_s are the resistances of the TES and the biasing shunt resistor, T and T_b are the TES and heat sink temperatures, and $(n - 1)$ is the exponent of the temperature dependence of G. For values of α typical of TES thermometers,

$$\tau_{\text{eff}} \sim \frac{\left(\frac{Cn}{\alpha G}\right)\left(1 + \beta + \frac{R_s}{R}\right)}{(1 - \frac{R_s}{R})(1 - \frac{T_b^n}{T^n})} . \qquad (2)$$

The easiest term to address is R_s, which was 0.5 mΩ, only about half of the TES resistance at the bias point. Dropping R_s to a still practical value of 0.2 mΩ will speed the recovery by a factor of ∼2. To achieve further reduction we will need to optimize G, C, and β. Because the extent of the linear range and τ_{eff} both depend on C/α, the the impact on linearity must be considered along with any possibility of reducing C. It should be possible to increase G by increasing the thickness of the silicon-nitride membrane. Thus far we have measured about the same value of G for 0.5 and 1.0 μm thick nitride at 0.09 K; it appears that G is at minimum in this thickness range,[12] so we are planning experiments with 2.0 μm thick nitride. We expect α and β to change when
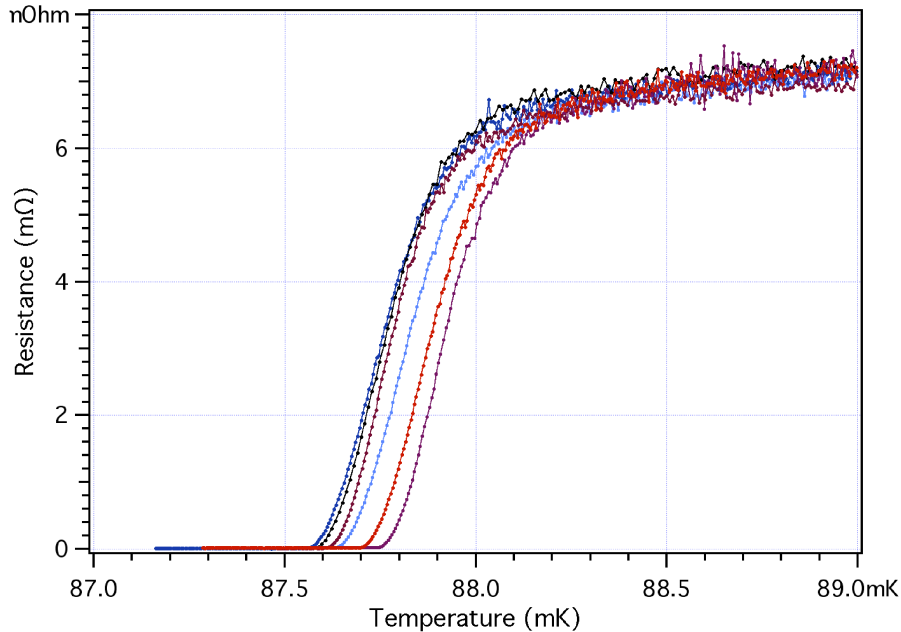
Figure 5. The superconducting transition shape for six TES sensors of one design. These transitions are all for TES's with a "T" shaped stem.

G is increased because these parameters depend on current, and with higher G more current is required to bias the TES at T_c. Thus we will need to reoptimize the design for higher G.

2.4 Array Uniformity

Uniformity of performance is paramount for future applications. As shown in Fig. 5, the shape of the superconducting transition in pixels of a given design is highly uniform (as long as the stray magnetic fields at the array are kept to $<\sim 1$ mG). These transition curves were determined from low-frequency (10 Hz) measurements of the transfer function of the TES as a function of temperature without any DC bias, using a very low AC bias current (< 10 nA) to ensure that there is no significant heating and that only a very small fraction of the transition region is sampled within each measurement. In normal operation the heat bath temperature is typically 50 mK, and our TES's are typically biased at $\sim 15\%$ of the normal resistance with a DC bias current of 50 μA. Under these conditions, the transition temperature is lowered by a few millikelvin, and the width of the transition is broadened.[13, 14] Thus, the uniformity of the transition when operated under the normal conditions for detecting x-rays is even more uniform than implied by Fig. 5.

Within an array that has stem designs of the "T" and "J" types randomly distributed, it has been found that "T" pixels systematically have a T_c that is 1.7 mK lower than the "J" pixels, resulting in a slight difference in the bias needed for the two types.[14] In terms of spectral resolution, both of these designs perform equally well at their respective optimal bias points. In Fig. 6 the uniformity of the optimal bias for four "T" pixels is shown. With a base temperature of 50 mK we measured the noise and pulse-shape for 5.9 keV Mn K$_\alpha$ x-rays, for a range of bias points between 7% of R_n and 35% of R_n. From the ratio of the signal to the noise at each frequency, we can determine the noise equivalent power (NEP). An integration of the NEP across all frequencies allows us to determine the achievable energy resolution,[15] assuming that the relation between the signal size and energy is linear, and it is this benchmark that is plotted in Fig. 6. Clearly the shape of these curves is very similar for all four pixels, indicating that a common bias can be used to obtain the optimal performance from all the pixels simultaneously. This figure also indicates that there is more than one minimum. Typically we have operated these devices at $\sim$15% of R_n, which is at the minimum in Fig. 6. However, we have also achieved excellent resolution from biasing as low as 7% of R_n. Operation at bias points so close to R_s can result in unstable behavior, thus the higher bias of 15% is preferred.
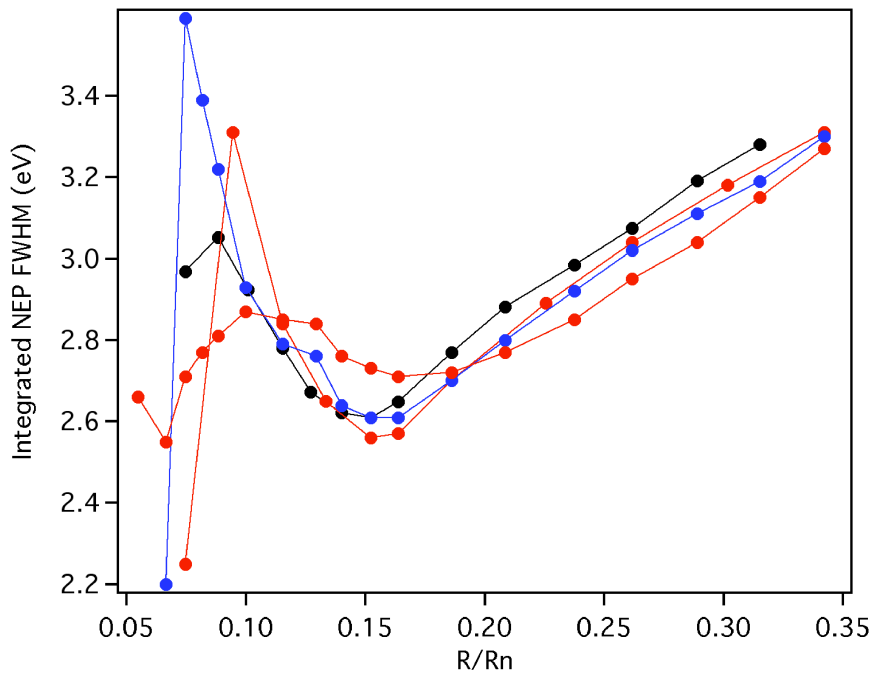
Figure 6. This figure demonstrates the uniformity of sensitivity of our TES pixels. The energy resolution that is determined from integrating the noise equivalent power is plotted as a function of the bias point. The bias point is displayed as the fraction of resistance at the TES (R) compared with the normal resistance of the TES (R_n). The bias resistance was determined assuming a constant relation between the bias current and bias resistance for all the pixels, based on the relationship determined for one pixel.
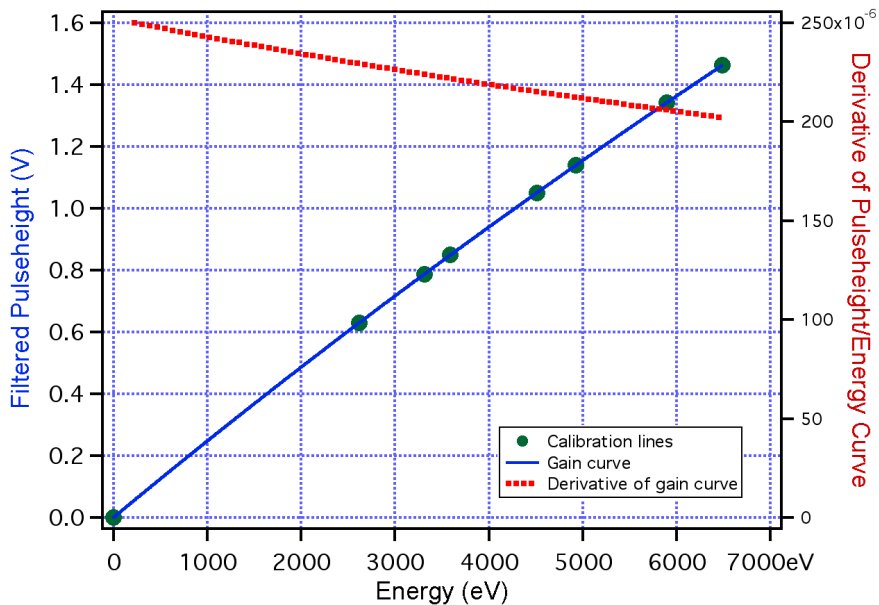

Figure 7. Relationship between the observed pulse height and the known energy deposited by x-rays from fluoresced targets. The points shown come from Mn K_α, Mn K_β, Ti K_α, Ti K_β, K K_α, K K_β, and Cl K_α.
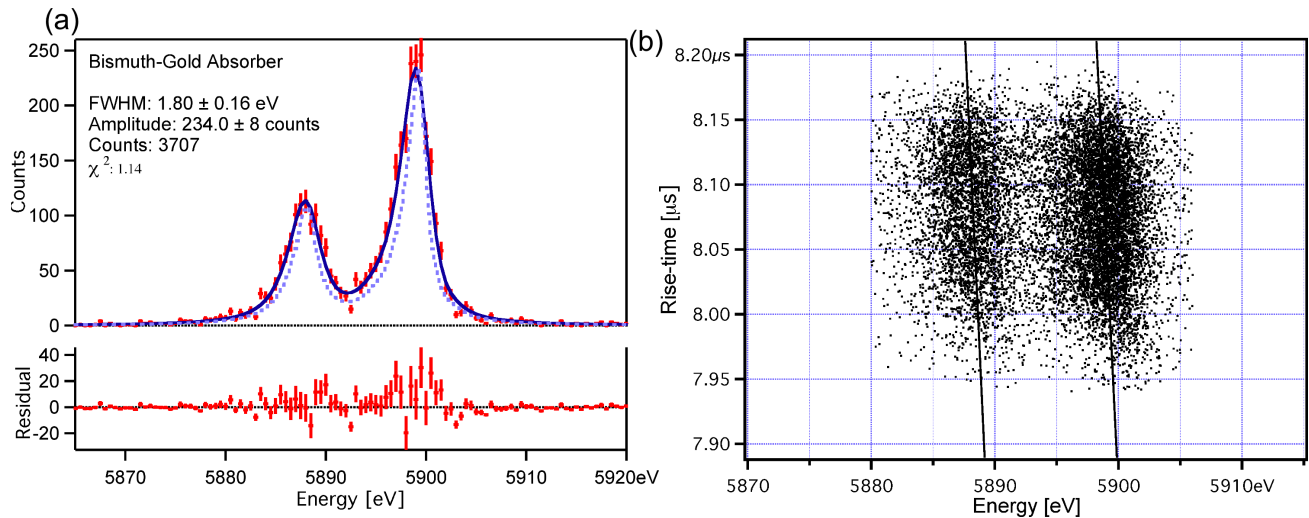
Figure 8. (a) A spectrum of Mn K$_\alpha$ x-rays from an ^{55}Fe source with one of pixels with a "T"-shaped stem and a BiAu absorber, with discrimination on TES temperature. The instrumental function is consistent with a Gaussian response with a resolution of 1.8 eV FWHM. The dashed line shows the intrinsic line shape from Hölzer et al.,[3] with correction and extension provided by Hölzer via private communication. (b) Plot of the pulse rise time versus pulse height for MnK$_\alpha$ x-rays before reducing the high-frequency cut-off, revealing a slight correlation.

The linearity of these detectors is shown in Fig. 7. We have plotted the pulse height as determined from an optimal digital filter as a function of energy. In general the filtered pulse height is typically a more linear function of energy than the raw pulse height.[16] The slope at the origin is less than 10% steeper than the slope at 6 keV, and therefore the use of the integrated NEP as an estimate of the resolution in a scan of biases voltages is valid.

3. GOLD/BISMUTH ABSORBERS

Using the combination of Bi and Au we can tune the heat capacity of the absorber over a wide range while maintaining a constant QE. In our first arrays using electroplated bismuth, we electroplated only 0.5 μm of Au on a 0.2 μm evaporated Au seed layer, then electroplated 6 μm of bismuth on top of the Au. These absorbers have a heat capacity of 0.4 pJ/K. The electroplated bismuth has larger grains (5-10 μm) and a factor of 10 lower electrical resistivity than our evaporated bismuth films. We measured 2.1 ±0.1 eV FWHM at 6 keV with such a device; the noise level and slope of the gain curve suggest that 1.6-eV resolution should be possible at low energies. When the data are screened such that events are kept only if they occur while the TES operating temperature is within a small acceptance range (as determined from the DC level of the signal current), leaving approximately one quarter of the total counts, the resolution improves to 1.8 ±0.2 eV FWHM at 6 keV, as shown in Fig. 8(a). The TES temperature is determined from the DC signal current just before the x-ray is absorbed. This exercise highlights both the high intrinsic resolution of the device as well as the need to improve upon the stability of the laboratory test platform if resolutions better than 2 eV are to be measured.

The first arrays we made using these new absorber designs were actually identical to the Au/Bi devices just described except that both the Au and Bi were evaporated. In that case, the resolution was no better than 4-eV FWHM, and the line shape was distinctly non-Gaussian, with a long shoulder to low energy.[2] Thus it is the combination of the novel absorber designs with the high-quality absorbers possible through electroplating that has been the critical breakthrough.

In Fig. 8(b) we show a plot of the rise time versus pulse height in the sensors with electroplated Au/Bi absorbers. There is a very slight negative correlation, indicating that the equilibration time in the absorber might not be completely negligible. The effect is removed by reducing the high frequency cut-off of the optimal filter to 10 kHz, without any significant loss of sensitivity. The Au of these devices had a residual resistivity

ratio of 7, which is 7 times lower than was achieved in the all-Au absorbers and in other electroplated 0.5 μm films.[5] With a higher conductivity Au layer in the Au/Bi absorber the equilibration will be faster.

The energy resolution of a TES generally scales as $T(C/\alpha)^{1/2}$, where T is the transition temperature and C is the heat capacity. Because a TES is linear over a small temperature range, there is a maximum allowable temperature change, and the device must be designed so that this temperature change corresponds to the maximum energy of interest. This results in an optimization in which C and α must be changed together. The choice of a particular combination of C and α is determined from materials properties, the energy range of interest, QE requirements, and the reproducibility of α. There is also the issue of whether the unexplained white noise endemic to existing TES devices is fundamentally a function of α (as determined empirically by Ullom[1]) or β (as calculated by Irwin for a non-Ohmic resistance near equilibrium[17]). Our TES bilayers show behavior[4] that agrees with both Irwin's calculation of the dependence of noise on β, and, within a single transition, Ullom's measured dependence on α. Independent of the fundamental origin, this noise term favors an optimization of C/α with the minimum C and α that can be achieved with an absorber than meets the other required properties. Thus, our future studies of Au/Bi absorbers will analyze the trade-off of minimizing the amount of Au to reduce heat capacity against keeping the thermal conductivity high enough to achieve the best energy resolution possible for different absorber geometries.

4. CONCLUSIONS

We have designed a novel way of attaching absorbers to TES sensors that allows the first layer of the absorber above the TES to have high electrical conductivity. This approach has allowed us to achieve breakthrough energy resolution of 2 - 3 eV at 6 keV in arrays using all-gold and gold-bismuth absorbers, as well as a high degree of uniformity. The success of replacing a fraction of the gold with electroplated bismuth now enables us to tune the heat capacity to suit other design criteria.

ACKNOWLEDGMENTS

REFERENCES

1. J. N. Ullom, W. B. Doriese, G. C. Hilton, J. A. Beall, S. Deiker, W. D. Duncan, L. Ferreira, K. D. Irwin, C. D. Reintsema, and L. R. Vale, "Characterization and reduction of unexplained noise in superconducting transition-edge sensors," *Appl. Phys. Lett.* **84**, pp. 4206–4208, 2004.

2. C. A. Kilbourne, S. R. Bandler, A. D. Brown, J. A. Chervenak, E. Figueroa-Feliciano, F. M. Finkbeiner, N. Iyomoto, R. L. Kelley, F. S. Porter, T. Saab, J. Sadleir, and J. White, "High-density arrays of x-ray microcalorimeters for Constellation-X," *Proc. SPIE* **6266**, pp. 626621–1 – 62662–9, 2006.

3. G. Hölzer, M. Fritsch, M. Deutsch, J. Härtwig, and E. Förster, "K$\alpha_{1,2}$ and K$\alpha_{1,3}$ x-ray emission lines of the *3d* transition metals," *Phys. Rev. A* **56**, pp. 4554–4568, 1997.

4. N. Iyomoto, S. R. Bandler, R. P. Brekosky, A. D. Brown, J. A. Chervenak, E. Figueroa-Feliciano, F. M. Finkbeiner, R. L. Kelley, C. A. Kilbourne, F. S. Porter, J. Sadleir, and S. J. Smith, "Modelling of TES x-ray microcalorimeters with a novel absorber design," in *Proceedings of 12th International Workshop on Low Temperature Detectors, Paris 2007, to be published in J. Low Temp. Phys.*, 2007.

5. A. D. Brown, S. R. Bandler, R. P. Brekosky, J. A. Chervenak, E. Figueroa-Feliciano, F. M. Finkbeiner, N. Iyomoto, R. L. Kelley, C. A. Kilbourne, F. S. Porter, J. Sadleir, and S. J. Smith, "Absorber materials for transition-edge sensor x-ray microcalorimeters," in *Proceedings of 12th International Workshop on Low Temperature Detectors, Paris 2007, to be published in J. Low Temp. Phys.*, 2007.

6. M. A. Lindeman, S. R. Bandler, R. P. Brekosky, J. Chervenak, E. Figueroa-Feliciano, F. Finkbeiner, M. J. Li, and C. A. Kilbourne, "Impedance measurements and modeling of a transition-edge-sensor calorimeter," *Rev. Sci. Inst.* **75**, pp. 1283–1289, 2004.

7. N. Iyomoto, S. R. Bandler, R. P. Brekosky, A. D. Brown, J. A. Chervenak, F. M. Finkbeiner, R. L. Kelley, C. A. Kilbourne, F. S. Porter, J. Sadleir, S. J. Smith, and E. Figueroa-Feliciano, "Close-packed arrays of transition-edge x-ray microcalorimeters with high spectral resolution at 5.9 kev," *submitted to Appl. Phys. Lett.* , 2007.

8. C. A. Kilbourne, S. R. Bandler, R. P. Brekosky, A. D. Brown, J. A. Chervenak, E. Figueroa-Feliciano, F. M. Finkbeiner, N. Iyomoto, R. L. Kelley, F. S. Porter, and S. J. Smith, "Various optimizations of x-ray TES arrays," in *Proceedings of 12th International Workshop on Low Temperature Detectors, Paris 2007, to be published in J. Low Temp. Phys.*, 2007.

9. C. K. Stahle, M. A. Lindeman, E. Figueroa-Feliciano, M. J. Li, N. Tralshawala, F. M. Finkbeiner, R. P. Brekosky, and J. A. Chervenak, "Arraying compact pixels of transition-edge microcalorimeters for imaging x-ray spectroscopy," in *AIP Conf. Proc.*, **605**, pp. 223–226, 2002.

10. H. F. C. Hoevers, M. L. Ridder, A. Germeau, M. P. Bruijn, P. A. J. de Korte, and R. J. Wiegerink, "Radiative ballistic phonon transport in silicon-nitride membranes at low temperatures," *Appl. Phys. Lett.* **86**, p. 251903, 2005.

11. K. D. Irwin and G. C. Hilton, "Transition-edge sensors," in *Topics in Applied Physics: Cryogenic Particle Detection*, C. Enss, ed., pp. 63–149, Springer-Verlag, Berlin, Heidelberg, 2005.

12. I. J. Maasilta and T. Kühn, "Effect of thin ballistic membranes on transition-edge sensor performance," in *Proceedings of 12th International Workshop on Low Temperature Detectors, Paris 2007, to be published in J. Low Temp. Phys.*, 2007.

13. M. A. Lindeman, K. A. Barger, D. E. Brandl, S. G. Crowder, L. Rocks, D. McCammon, and H. F. C. Hoevers, "The superconducting transition in 4-d: temperature, current, resistance and heat capacity," in *Proceedings of 12th International Workshop on Low Temperature Detectors, Paris 2007, to be published in J. Low Temp. Phys.*, 2007.

14. S. J. Smith, S. R. Bandler, A. D. Brown, J. A. Chervenak, F. M. Finkbeiner, N. Iyomoto, R. L. Kelley, C. A. Kilbourne, F. S. Porter, and J. Sadleir, "Characterizing the superconducting-to-normal transition in Mo/Au transition-edge sensor bilayers," in *Proceedings of 12th International Workshop on Low Temperature Detectors, Paris 2007, to be published in J. Low Temp. Phys.*, 2007.

15. S. H. Moseley, J. C. Mather, and D. McCammon, "Thermal detectors as x-ray spectrometers," *J. Appl. Phys.* **56**, pp. 1257–1262, 1984.

16. S. R. Bandler, E. Figueroa-Feliciano, N. Iyomoto, R. L. Kelley, C. A. Kilbourne, K. D. Murphy, F. S. Porter, T. Saab, and J. E. Sadleir, "Non-linear effects in transition edge sensors for x-ray detection," *Nucl. Inst. and Meth. A* **559**, pp. 814–817, 2006.

17. K. D. Irwin, "Thermodynamics of nonlinear bolometers near equilibrium," *Nucl. Inst. and Meth. A* **559**, pp. 718–720, 2006.